Measurement of Airborne Ultrasound Focus on Skin Surface Using Thermal Imaging

Ryoya Onishi , Sota Iwabuchi , Shun Suzuki , Takaaki Kamigaki , Yasutoshi Makino ,
and Hiroyuki Shinoda , *Member, IEEE*

Abstract—In recent years, tactile presentation technology using airborne ultrasound has attracted attention. To achieve an ideal tactile presentation using ultrasound, the acoustic field on the user's skin surface must be determined, particularly the location of the focal point. Previous studies have suggested that thermal images can be used to immediately visualize sound pressure patterns on finger surfaces. In this study, we comprehensively investigated the performance of thermal imaging for measuring the ultrasound focus on the skin. First, we confirmed that the sound pressure peak at the focus and the temperature change peak were matched using silicone that mimicked the skin. In addition, we confirmed that when human skin was irradiated, a temperature increase was observed at above 4.0 kPa in 9 out of 10 participants. Moreover, a 5.5 kPa focus could be employed to track the focal position. if the moving velocity was less than 100 mm/s and to detect the orbit if the velocity was less than 2000 mm/s. These results clarify the situation in which the focus can be measured by using thermal images and provide guidelines for practical use.

Index Terms—Measurement, mid-air haptics, thermography, ultrasounds.

I. INTRODUCTION

IN RECENT years, mid-air haptics, a tactile presentation technology that uses airborne ultrasound, has attracted significant attention [1], [2]. Using the radiation pressure of airborne ultrasound, users can perceive a noncontact tactile sensation without attaching devices. Ultrasound-phased arrays can produce the desired pressure pattern with high spatiotemporal resolution and reproducibility [3], [4]. This technology has been used in several studies, including its application to tactile interfaces [5], [6], [7], [8], [9], [10], [11], [12], [13] and to elucidate the tactile perception in mid-air haptics, the focal point measurement of the skin surface is essential. Misalignment of

the focal position or force presentation position alters the tactile sensation. Moving focal points have widely been used to present strong vibration and pressure sensations [14], [15], [16], [17], [18], [19], and changing the trajectory of the moving focal point results in a different tactile sensation. In addition, changes in the speed of sound, which depends on the temperature and humidity, and interference with the sound field by surrounding objects, including the user, can cause focal point shifts.

Although visualization with alternative irradiation targets such as oil baths [20] and user sensory evaluation have been used to clarify the focal point position, the focal position on the skin surface needs to be directly measured. Additionally, ultrasound waves cannot be perceived with eyes or ears, and the operator cannot notice the cessation of irradiation due to malfunction or misalignment of the irradiation position due to programming errors; thus, physical measurements are required even during the experiment. However, measuring the focal position of the finger surface by employing common measurement methods is difficult. Microphones themselves interfere considerably with the sound field, and it takes an enormous amount of time to scan the microphones to identify the focal point. Furthermore, optical measurements, such as schlieren, are not possible because the light path is obstructed by the finger itself.

A method for measuring the sound pressure from reflected waves, proposed in 2021 [21], can identify the focal position on the surface; however, it has been suggested that the measurement performance depends on the normal direction of the target surface. In 2022, the visualization of the acoustic field on the skin from thermal images was proposed [22]. This is based on the phenomenon in which a temperature increase occurs at a high-sound-pressure location, such as a focal spot, on the surface of an object. Based on this study, we previously evaluated the performance of focus measurements using thermal images [23]. However, the evaluation was conducted under limited circumstances using only an unmodulated focus and a specific type of stick-shaped irradiation target. Therefore, the scope of measurement applications should be expanded and a more detailed investigation for practical use conducted.

First, using a silicone rubber sheet with a hole and a microphone attached to its back, we verified the difference between the sound pressure distribution and the temperature change distribution on a flat surface. It was confirmed that the sound pressure distribution obtained by two-dimensional scanning of the sheet with an automated stage and the temperature change distribution

matched with an error of less than 1 mm, independent of the angle between the beam and sheet. Through experiments in which the focal point was scanned along the surface, it was confirmed that the sound pressure and temperature peaks matched within 2 mm accuracy even if the surface was curved in shape. Through experiments in which the focal point was shifted perpendicular to the surface, we confirmed that the position with the most significant temperature change and the position with the most enormous sound pressure were within 10 mm of each other.

Next, we clarified the measurement limits of sound pressure at the focus when the amplitude was modulated or unmodulated. Considering differences in skin surface conditions such as sweat and body temperature, we observed temperature changes when ultrasound was irradiated on the fingers of 10 participants. At the unmodulated focus, measurement was possible if the root mean square (RMS) sound pressure was 4.0 kPa. When the amplitude was modulated with a sinusoidal wave on the finger of one of the participants, even an RMS sound pressure of 3.08 kPa, which is the maximum output, could not be measured. Meanwhile, when amplitude modulation was applied with a square wave, it was confirmed that measurement was possible with a duty ratio of 55% or more, with an RMS pressure of 4.1 kPa or more. These results imply that a focus with an RMS value of 4.0 kPa should be used for the application of thermal imaging.

Finally, the measurement performance of the moving focus in the spatial modulation was evaluated. A moving focus was visualized for the 5.5 kPa focus if the movement speed was less than 100 mm/s. At higher velocities, the location of the moving focus could not be detected, although the trajectory of the moving focus could be seen at velocities below 10000 mm/s.

These results will be helpful for researchers and developers who utilize ultrasound measurements using thermographic imaging. This allows the ultrasound focus to be presented at the desired location and enables highly reproducible airborne tactile presentation. In addition, any shift in the focus position or cessation of output owing to malfunction can be immediately detected. The ability to compensate quickly and accurately for the spatiotemporal modulation of the focal point on the skin surface is also expected to enable a tactile experience with a higher perceived intensity.

II. Principle

The focal position can be measured based on the phenomenon that, when high-intensity airborne ultrasound is irradiated, a temperature rise occurs on the object surface at positions of high sound pressure [22]. In this study, we measured the skin temperature using a thermography camera. By using thermography, it is possible to measure the temperature non-contactly, allowing the sound pressure at the focal point to be measured without disturbing the sound field. Previous efforts to enhance the accuracy of thermography have included algorithm improvements [24] and investigations into the effects of substances adhered to the surface [25]. Thermography technology has been utilized for various applications, such as estimating biological information from skin temperature [26], [27]. Consequently, the temperature change peak at the ultrasound focus aligns with the sound pressure peak, particularly at the ultrasound focus. To measure the deviation between the peak positions of sound pressure and temperature change, we used a microphone-attached silicone mimicking the finger or palm shape. This enabled determining the ultrasound focal position on the finger by assessing the temperature change peak. Although the specific mechanism and formula for the temperature increase remain unclear, the study's primary goal is to identify the "position" of the focal point. Quantitative evaluation, involving sound wave air attenuation and compression energy proportional to the square of the sound pressure is beyond the study's scope.

III. Experiment 1: Object Scanning to Compare the Sound Pressure Distribution and Temperature Change Distribution.

We confirm that the peak position of the temperature increase at the surface of the object corresponds to the focal point. The distributions of the sound pressure and temperature changes were compared for a silicone plate when a focal point was generated on the surface of the silicone plate. The difference at the peak position corresponds to the accuracy of measuring the focal point from the temperature peak. A hole was drilled in the center of the silicone plate, and the sound pressure was measured using a microphone attached to the back of the silicone plate. The sound pressure distribution on the plane was acquired by scanning a flat silicone plate in two dimensions using an automatic stage. The silicone plate was then replaced with another silicone plate without holes, and the two-dimensional distribution of the temperature change was acquired using a thermography camera to detect the peak temperature position.

A. Procedure

A photograph of the experimental setup is shown in Fig. 1. The setup consisted of six ultrasound phased arrays, a thermographic camera (OPTPI 45ILTO29T090, Optris), a silicone plate with holes, and a microphone attached to the back. The phased-array hardware and software were AUTD3 [28]. The resolution of the thermographic camera was 382×288 px, and the sensitivity was 40 mK. A silicone plate with holes was ground to the XYZ autostage and scanned in two dimensions. The angle of the silicone plate was controlled using a rotary table (Fig. 1(b)). The size of the silicone plate was $100 \times 90 \times 5$ mm, which was sufficiently more significant than the area to be scanned. To measure the sound pressure on the surface, a 0.5 mm hole was drilled, an ultrasound transducer (MA40S4R) was attached to measure the sound pressure, and an oscilloscope (PicoScope 2205MSO, Pico Technology) was used to obtain sound pressure information. The room temperature and humidity during the experiment were $22.4°C$ and 43.5%, respectively.

B. Results

Fig. 2 shows the sound pressure distribution obtained from the stage scan during focus generation and the temperature change
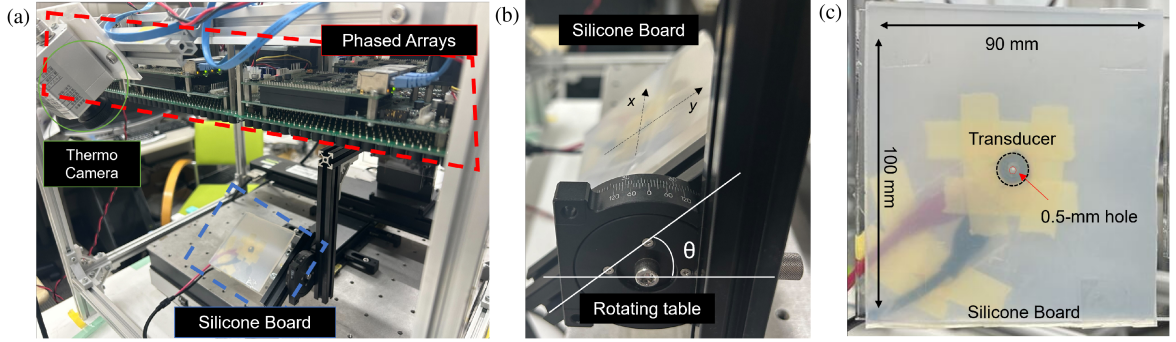
Fig. 1. (a) Photograph of the experimental setup, consisting of six ultrasound phased array units, a thermographic camera, and a silicone plate with a microphone attached to the backside. The distance between the position of the holes in the silicone and the phased array is 229 mm. (b) Photograph of the silicone plate mounted on a rotating stand, the angle of which can be freely changed by the rotating stand. $theta = 0°$ is when the plate is horizontal to the phased array. (c) Enlarged view of the silicone plate. A hole is drilled in the center of the silicone plate to measure the sound pressure with a transducer attached to the back side.
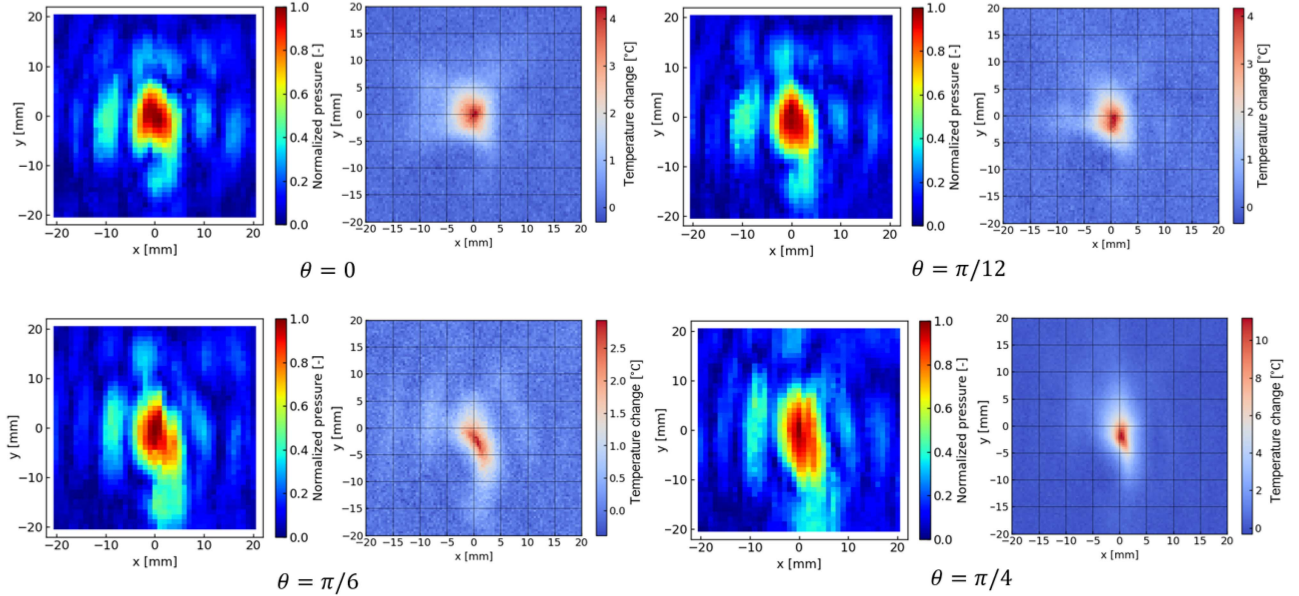

Fig. 2. Image plots of sound pressure distribution and temperature distribution at the focus at different angles.

TABLE I
PEAK DISPLACEMENT MEAN STANDARD DEVIATION

angle	Pressure peak [mm]	Temp peak [mm]	Displacement [mm]
0°	(1.0, 1.0)	(0.1, 0.24)	(0.9, 0.76)
15°	(0.0, -0.97)	(0.1,-0.11)	(0.1, -0.86)
30°	(0.0, 0.0)	(0.3, -1.4)	(0.3, 1.4)
45°	(0.0, 0.0)	(0.1, -0.78)	(0.1, 0.78)

distribution after 5 seconds, obtained using the thermography camera. The center position of the focal point coincided at each angle and that the shapes of the focal points, including the side lobes, were consistent. Table I lists the positions that take maximum pressure and temperature change at each angle. These results confirmed that the focal center position can be measured from the temperature change distribution on the object surface with an accuracy of less than 1 mm.

IV. EXPERIMENT 2: FOCUS SCANNING TO COMPARE THE SOUND PRESSURE DISTRIBUTION AND TEMPERATURE CHANGE DISTRIBUTION

A. Procedure

Scanning the irradiated object in two dimensions while fixing the focus generation position, as in Experiment 1, did not correspond to the sound pressure distribution on the surface depending on the shape of the object. For the same reason, the method used in Experiment 1 cannot be applied when examining the shift of the focus in the z-direction, regardless of the shape, because the sound field changes significantly. Therefore, the silicone is fixed, and the focal point is scanned to check whether the temperature increase reaches its maximum value when the sound pressure reaches its maximum value. The sound pressure obtained using a microphone attached to the back side of the silicone material with a hole drilled into it, the
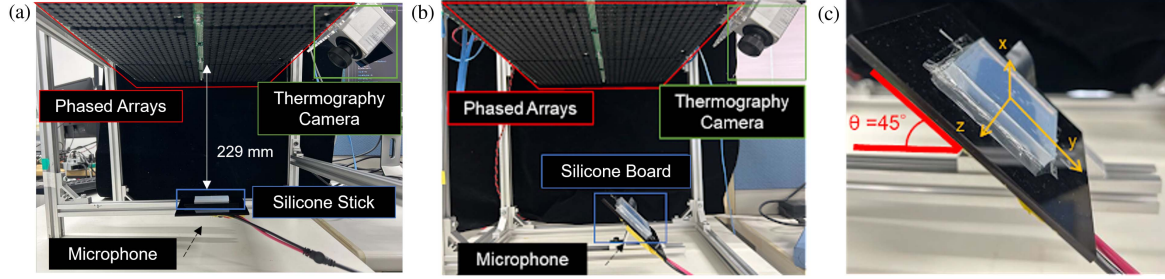
Fig. 3. Experimental setup consists of six ultrasound phased array units, a thermographic camera, and (a) a silicone stick, which is a finger model, or (b) a silicone plane, which is a palm model, with a microphone attached to the backside. The distance between the location of the hole in the silicone and the phased array is 229 mm. (c) Peak comparison experiments are performed with the flat plate placed horizontally to the phased array at $theta = 0°$ and at an angle of $theta = 45°$.
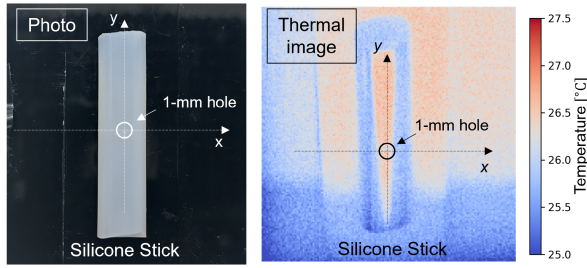

Fig. 4. Comparison of a photo of a silicone stick with a thermal image. Sound pressure was measured by using a microphone mounted behind the stick.

Fig. 5. Thermal images when the focus is moved 2 mm along the x axis. The x coordinates [mm] and normalized squared sound pressure p^2 [-] are shown below each image. Thermal images when the focus is moved 2 mm along the x-axis. The x coordinates [mm] and normalized squared sound pressure p^2 [-] are shown below each image.

temperature change at the position of the hole, and the peak positions were compared. Fig. 3 shows a photograph of the experimental setup. The setup was the same as that used in Experiment 1; however, the irradiation target was replaced with a silicone stick (12 mm in diameter) as a dummy finger and a silicone plate ($50 \times 50 \times 5$ mm) as a dummy palm, which mimics the shape of a human finger. The silicone stick and the silicone plate each had a 1 mm hole and were measured with a microphone.

The focal point was moved at 0.5 mm intervals in the x, y-directions (horizontal to the surface) and in the z direction (vertical to the surface). Ultrasonic irradiation was performed for 0.6 s. This trial was conducted five times in the x, y, and z directions. In this experiment, the amplitude of each ultrasound transducer was limited to 58% of its maximum value, considering the upper measurement limit of the microphone. Fig. 4 presents a photograph of the silicone stick and its thermal image. The shape of the silicone stick is observed in the thermal image. During the x-axis experiment, the room temperature and humidity were 20.4°C and 41.6%, respectively. During the y-axis experiment, the room temperature and humidity were 26.9°C and 17.9%, respectively; in the z-direction, these were 23.7°C and 68.5%, respectively. In the x-axis, the temperature and humidity were 23.9°C and 35.1% for the x, y, and z-axis when the plane was 0°, and 22.2°C and 40.0% for the x-, y-, and z-axis when the plane was 45°.

B. Results and Discussion

Fig. 5 shows the temperature distribution after 0.5 s when the focal point was moved at 2 mm intervals. We identified the focal
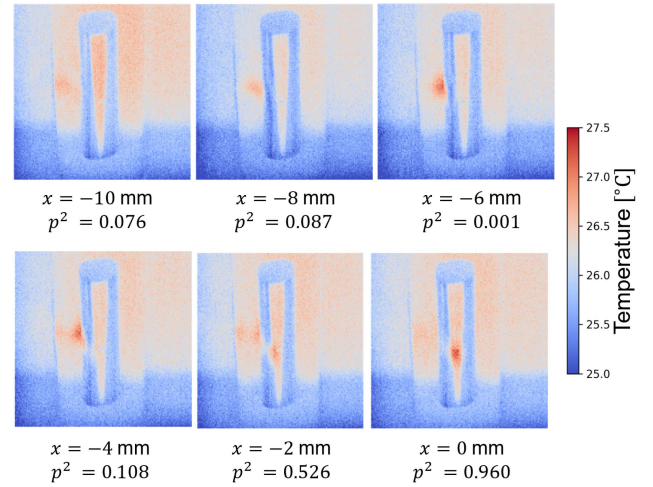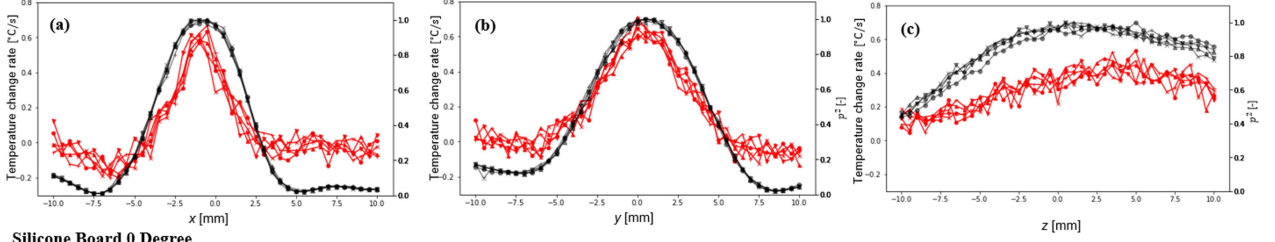
point in the thermal image and observed that the temperature peak shifted according to the irradiation position.

Fig. 6 depicts the temperature change and normalized squared sound pressure at the microphone hole when the focal point was shifted by 0.5 mm in the x-, y-, and z-directions, respectively. The point with the highest sound pressure or temperature change and its eight neighboring points were each fitted with a quadratic function to calculate the deviation between the temperature change and the sound pressure peak. Table II summarizes the

TABLE II
PEAK DISPLACEMENT MEAN STANDARD DEVIATION

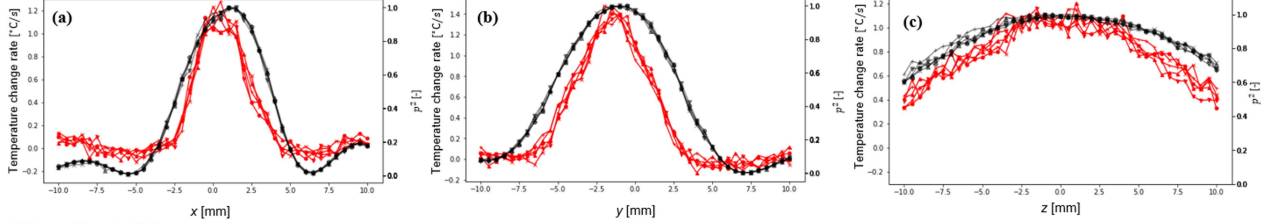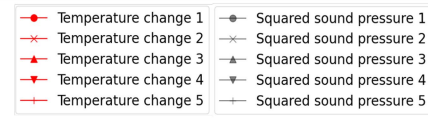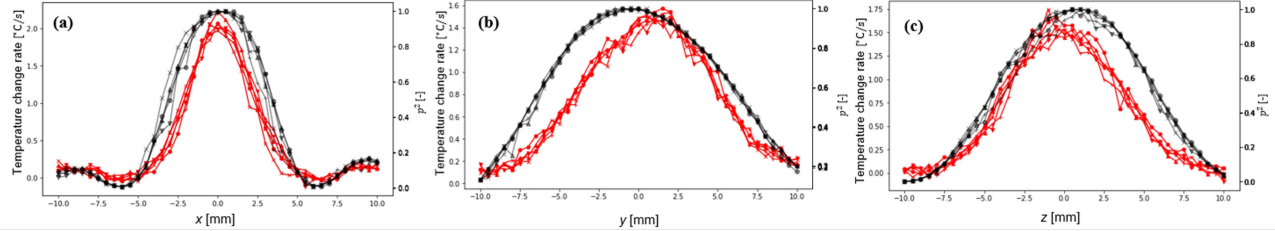| Axis	Peak Displacements [mm]	Mean [mm]	SD [mm]
Cylinder x	0.12, -0.26, 0.01, -0.28, 0.10	0.06	0.19
Cylinder y	-0.32, -0.26, 0.09, -0.20, -0.38	-0.25	0.11
Cylinder z	0.50, 3.72, 2.44, 2.23, 2.61	2.30	1.16
Plane x	-0.55, -0.37, -0.36, -0.57, -0.56	-0.48	0.11
Plane y	-0.38, 0.27, -0.37, -0.33, -0.34	-0.23	0.28
Plane z	-0.81, -0.03, 0.29, -1.33, -0.60	-0.49	0.64
Slope x	-0.19, -0.06, 0.03, -0.06, 0.11	-0.03	0.11
Slope y	1.65, 0.95, 1.43, 1.88, 1.61	1.50	0.35
Slope z	-1.42, -0.99, -1.00, -0.62, -1.33	-1.07	0.32

Fig. 6.   Simultaneous plots of temperature change rate and sound pressure at silicone stick, silicone plate $0°$ (Plain), and silicone plate $45°$ (Slope) when the focus is scanned in (a) x, (b) y, and (c) z directions. The temperature change rate was measured from thermal images taken with a thermographic camera, and the sound pressure was measured with a microphone attached to the back of the hole. The cylinder and plain models' temperature change, sound pressure distribution, and peaks match well. On the other hand, there is a slight deviation for the slope model, with a deviation of about 1.5 mm in the y direction.

deviations, means, and standard deviations of the temperature change and sound pressure peaks.

The results confirm that the peak positions of the sound pressure and temperature coincide regardless of the shape. For cylinders and planes at $0°$, the agreement is accurate within 0.5 mm. Fig. 6 also reveals that the shapes of the distributions match. This implies the possibility of accurately measuring the center of the focus.

In the z direction (normal to the cylinder), the peak position was off by 2 mm, which is a larger error than that in the x- and y-directions (tangential to the cylinder). A possible reason for this is the effect of acoustic streaming. When the focal point was placed in front of the irradiation target, acoustic streaming had a cooling effect. The peak position of the temperature shifted back to the back of the target owing to acoustic streaming. However, even if the focal point is shifted 2 mm in the z-direction, the sound pressure is more than 96 % of the maximum sound pressure, so if there is no shift in the x- and y-direction, it is sufficient for calibration in tactile presentation. In the y direction of the slope, there was a positional deviation of 1.5 mm. The cause of the positional deviation is thought to be acoustic streaming as well as the effect of viscous heating that depends on the angle between the ultrasonic beam and the target surface. This

dependence of accuracy on angle can be a limitation of this method.

V. Experiment 3: Focus Measurement by Thermal Images of a Human Finger

A. Procedure

We verify that sufficient temperature changes occur at the focal point formed on the actual finger. The thermal response of a finger may differ from that of a silicone stick, owing to the effects of perspiration and blood flow. Therefore, we confirmed that moving the focal point also moves the peak temperature position in the thermal image. In the experiment, we irradiated the index finger with an ultrasound focus and observed the temperature change. The room temperature and humidity during the experiment were $25.5°C$ and 37.3%, respectively.

B. Results and Discussion

Fig. 7 shows the temperature change at 0.5 s after irradiation. The peak position of the temperature increase shifts according to the focal position.
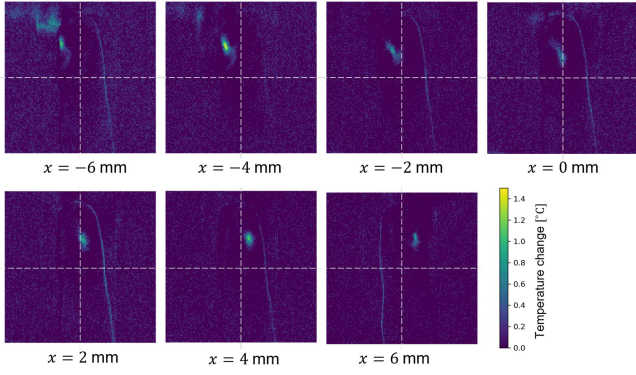
Fig. 7. Images of temperature change when a focal point is generated on the finger surface. The focal point was shifted by 2 mm in the x -axis direction from the finger center position, suggesting that the temperature change image after 0.5 s reflects the focal position.
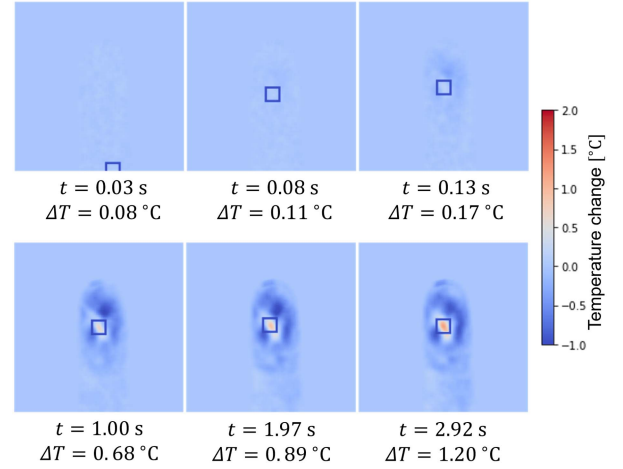

Fig. 8. Estimated focal point at each time. The central square boundary represents the focal point. The thermal image shows the temperature increase from $t = 0$. ΔT is the temperature increase at the estimated focal position.

In this experiment, we used six units of ultrasound-phased arrays to produce a focal point of high sound pressure to induce a significant temperature increase. Thermal imaging cannot be used to measure normal-intensity sound pressures because of their low signal-to-noise ratios. However, they can be applied to the high sound pressures used in haptic applications.

VI. EXPERIMENT 4: FOCUS DETECTION ACCURACY AND MEASUREMENT TIME

A. Procedure

We investigated the relationship between the precision of the focal position measurement and the measurement time. Ultrasound was used to irradiate the author's finger instead of silicone in the same setup described in Experiment 3. The trials were repeated 30 times with ultrasound focused on the surface of the finger for 4 s. The finger was fixed in the same position during the experiment. The room temperature and humidity were 20.4°C and 41.6%, respectively. The estimated focal position was defined as where the largest temperature increases occurred. Note that the finger area was defined as the area where the temperature at the start of irradiation was 34°C or higher. We applied a 5-pixel × 5-pixel averaging filter to the thermal image to remove noise. One pixel in the thermal image corresponds to 0.39 mm.

B. Results and Discussion

Fig. 8 shows the images of the temperature change from $t = 0$. The estimated focal point is indicated by a blue box. The area was 150-pixel × 150-pixels and shows images of the temperature change in the first three frames after the start of irradiation and after 1, 2, and 3 s.

The time-series data for the estimated focal positions are shown in Fig. 9. The estimated position, that is, the position of the highest temperature, is plotted in different colors for 29 trials. One trial in which the temperature could not be measured correctly because of the automatic calibration of the thermographic camera is excluded. The estimated focal position converges over

time. The average of the estimated positions over 2 s < t < 3s, that is, the converged position, is set to x=0 and y=0. Fig. 9 displays that the focus is identified with a precision of 1mm in 0.2 s.

VII. EXPERIMENT 5: LOWER LIMIT OF FOCUS MEASUREMENT WITH AND WITHOUT MODULATION

The focal point can be measured if the temperature increase due to the ultrasound is sufficiently larger than the noise of the thermographic camera and the temperature fluctuation at the skin surface. Therefore, if the ultrasound power is reduced to a weak force or if the amplitude is modulated, to present a vibration sensation, the temperature change decreases; thus, focus measurement becomes difficult. We evaluated the measurement limit of when the sound pressure changes and when amplitude modulation is applied.

A. Procedure

First, we evaluated the focal point measurement when the output was varied based on the static pressure. The experimental environment was identical to that used in Experiment 3, with the finger placed in the silicone position, as shown in Fig. 3, and irradiated with ultrasound. In the experiment, the finger was fixed to avoid movement. A focus was generated at the center of the finger pad of the right hand, and the temperature distribution on the surface was acquired using a thermographic camera. The presentation position of the focal point was corrected in advance using thermal images such that it coincided with the center of the finger pad of the index finger. Time-series data of the sound pressure and temperature changes at the center of the finger pad were obtained when the sound pressure at the focal point varied from 2.3 kPa to 4.0 kPa. Considering the individual differences in the thermal properties of the skin, experiments were performed on ten participants (male: 7, female: 3, average age: 26.1 years, SD: 3.05, minimum age: 23, maximum age: 32) .
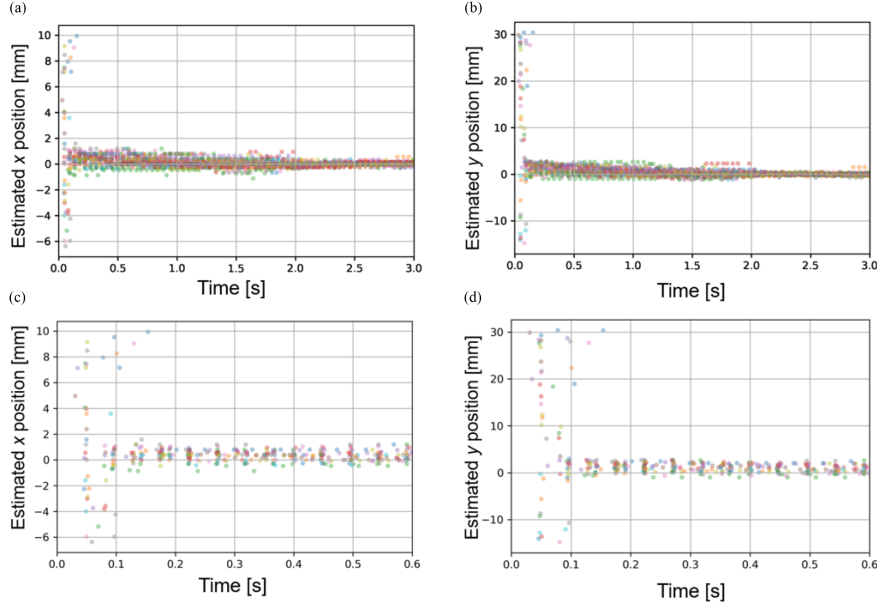
Fig. 9.   Time series data of the estimated focal point, where a and b represent the time variation of the estimated focal point along the x-axis and y-axis, respectively. The 29 trials are plotted in different colors. Moreover, c and d are enlarged views of a and b, respectively.

Furthermore, the focus measurements were evaluated when amplitude modulation was applied. The RMS value of the static pressure before amplitude modulation was 5.5 kPa. Three modulation frequencies were used: 10, 50, and 200 Hz. First, time-series data of the temperature at the center of the finger pad were obtained by amplitude modulation in the form of a sinusoidal waveform. This experiment was performed on the right hand of one of the participants (Participant 1), and irradiation was repeated 10 times under the same conditions for each frequency. Next, temperature time-series data were obtained using rectangular waveform amplitude modulation. The duty ratio of the rectangular waveform varied from 0.5 to 1.0, and irradiation was performed once for each.

B. Results and Discussion

Fig. 10(a) shows a time-series plot of the temperature change due to irradiation at each sound pressure when static pressure is used. Owing to the specifications of the thermography camera, the temperature is periodically calibrated and corrected to obtain accurate temperatures. A sufficient temperature increase is observed when the sound pressure at the focal point is 4.0 kPa in 9 out of 10 participants.

From Fig. 10(a), we observe that some people's temperature increases and others decrease even at the same sound pressure level. This is thought to be due to individual differences in the condition of the skin surface, especially in the amount of perspiration. It has already been reported that high humidity on the skin surface causes a temperature decrease [29]. One limitation of this method is that measurement limits can vary due to environmental and individual differences. For example, a high room temperature may increase sweating, causing different temperature behavior.

To clarify the relationship between measurement time and signal-to-noise (SN) ratio of acoustic pressure, we analyzed the experimental results of 10 participants shown in Fig. 10(a). Fig. 10(a) shows the temperature rise after ultrasound irradiation. We calculated the minimum observation time to detect this temperature increase using the following procedure. First, we assume that the ultrasonic irradiation start time t_0 is known and that the true temperature change due to ultrasonic irradiation is given by $T(t) = at + T(t_0)$ in a short interval $[t_0, t_0 + \tau]$. Second, we assume that the measured temperature is the linear summation of the above true value and noise; thus, the slope obtained by fitting a linear function to the data in the interval τ provides the best estimate of a. Under these assumptions, Fig. 10(b) provides the minimum measurement time required for ensuring 10 dB SN ratio for each participant. The horizontal lines are the temperature rise slope values of a around t_0 evaluated from the whole data of 0.5s, for each sound pressure level, ranging from 2.3 kPa to 4.0 kPa. Meanwhile, even in the absence of irradiation, the estimated value of a from a limited data of short interval τ does not equal zero due to noise. The standard deviation $\sigma(\tau)$ of this quantity provides the inevitable estimation error of a. In each graph of Fig. 10(b), a curve of $\sqrt{10}\sigma(\tau)$ that is 3.16 times the inevitable measurement error of a for measurement interval of τ is drawn for each participant. The $\sigma(\tau)$ was evaluated from the experimental data without ultrasound irradiation. If the true value of slope a is larger than $\sqrt{10}\sigma(\tau)$, it means that the slope can be measured more than 10 dB SN ratio for observation time τ. Alternatively, if a is given first, then τ that satisfies $\sqrt{10}\sigma(\tau) = a$ represents the minimum time for securing 10 dB SN ratio. For example, in the graph of Participant 1 in Fig. 10(b), the $p = 2.3$ kPa line intersects with $\sqrt{10}\sigma(\tau)$ at $\tau = 0.42$ s, which means at least 0.42 s is necessary to detect 2.3 kPa sound pressure with 10 dB SN ratio. Note that for $p = 4.0$ kPa in P1, the
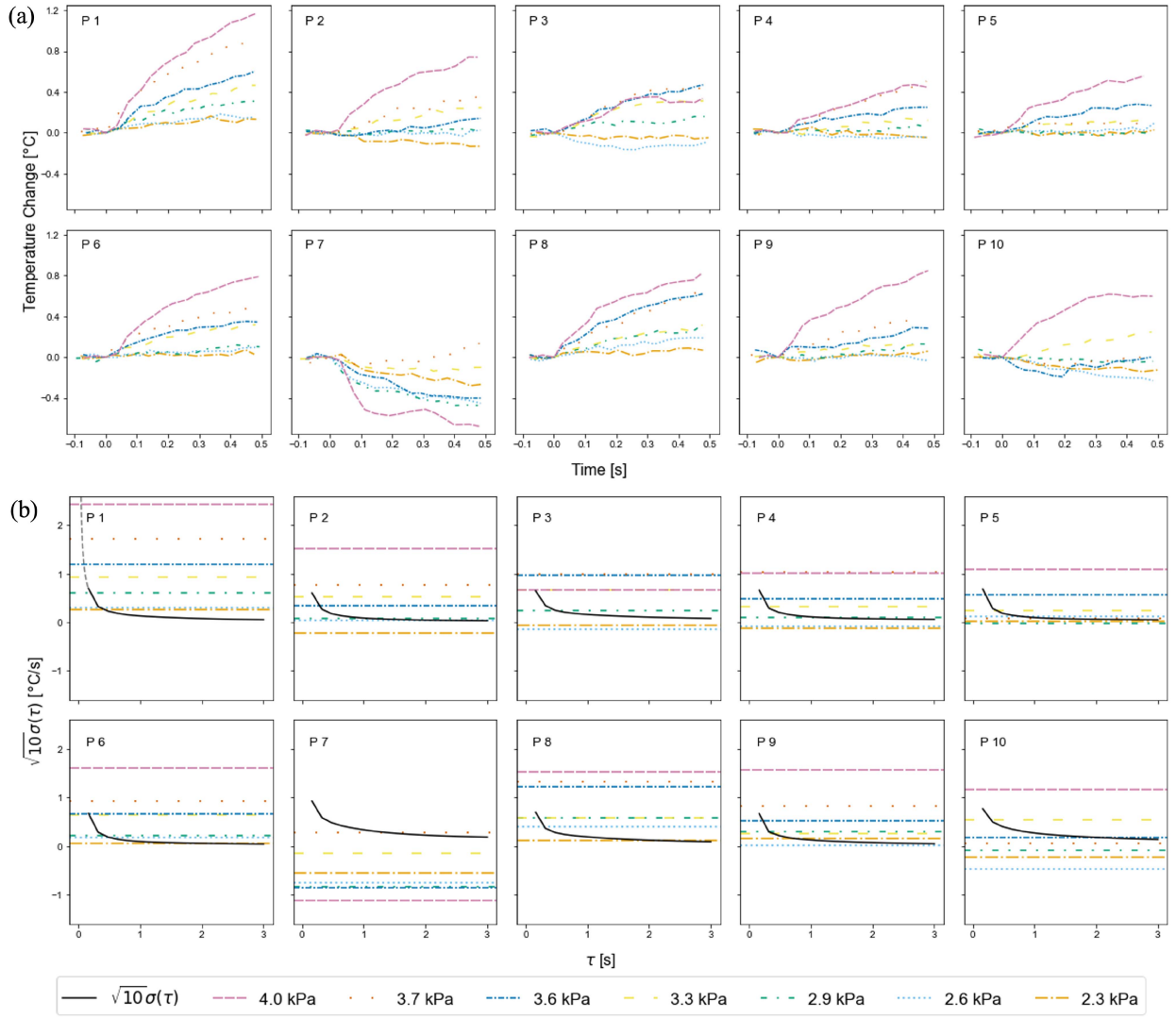
Fig. 10. (a) Plot of temperature change when ultrasound is irradiated to finger. The vertical axis represents the temperature change and the horizontal axis represents the elapsed time after the start of ultrasound irradiation. Plots were drawn for 10 participants (P1 - P10) individually. The different types of lines represent the RMS value of sound pressure. (b) The estimated a at each sound pressure level from 2.3 kPa to 4.0 kPa as a horizontal line, and a curve with $\sqrt{10}\sigma(\tau)$ for a signal-to-noise ratio of 10 dB. The intersection point represents the minimum detection time. Note that in the graph of P1, there is an extrapolation line obtained by fitting $\sigma(\tau) = A\tau^{-\beta}$.

horizontal line did not intersect with $\sqrt{10}\sigma(\tau)$ due to the frame rate limit of the thermography camera; therefore, we extrapolated the curve of $\sigma(\tau)$ by $A\tau^{-\beta}$ ($A = 0.1008$, $\beta = 1.1424$) to obtain the intersection point at $\tau = 0.06$ s. The minimum detection time for each subject obtained by the same procedure is summarized in Table III. The "-" denotes that a never exceeds $\sigma(\tau)$ within the assumed observation time of 30 s, meaning that it is undetectable. Table III indicates that focus irradiation can be measured within 0.16 s at 4 kPa for 9 out of 10 participants.

Next, we discuss the results of the modulated-focus measurement. Fig. 11 depicts the temperature change at each of the 10 modulation foci in a sinusoidal waveform. The 10 Hz results show that the temperature tends to increase with irradiation. At 50 and 200 Hz, a trend of temperature increase was also observed; however, in some cases, the temperature decreased. These results suggest that a stable measurement is difficult with

TABLE III
TIME REQUIRED FOR ULTRASOUND DETECTION [S]

	2.3 kPa	2.6 kPa	2.9 kPa	3.3 kPa	3.6 kPa	3.7 kPa	4.0 kPa
P1	0.42	0.33	0.18	0.13	0.11	0.10	0.06
P2	-	2.04	1.09	0.18	0.25	0.14	0.09
P3	-	-	0.47	0.16	0.12	0.12	0.16
P4	-	-	1.30	0.28	0.20	0.11	0.12
P5	-	0.84	-	0.36	0.17	1.48	0.11
P6	2.06	0.53	0.42	0.16	0.16	0.13	0.09
P7	-	-	-	-	-	1.31	-
P8	2.24	0.27	0.19	0.18	0.11	0.10	0.10
P9	0.71	-	0.31	0.37	0.19	0.14	0.09
P10	-	-	-	-	0.27	1.92	0.11

* - indicates a does not exceed $\sigma(\tau)$.

a sinusoidal modulation focus because the temperature increase is hidden in the noise.

Finally, Fig. 12 presents the results of the temperature change when amplitude modulation is applied to the rectangular
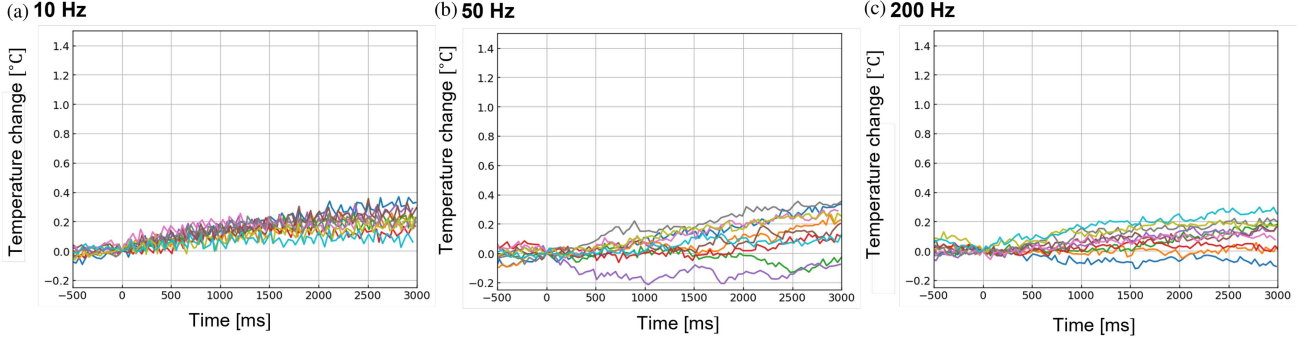
Fig. 11. Temperature change at the focal position in sinusoidal amplitude modulation. Ultrasound was irradiated at $t = 0$ s. The modulation frequencies were (a) 10 Hz, (b) 50 Hz, and (c) 200 Hz. The experiment was repeated 10 times under the same conditions for each frequency. The 10 results are plotted in the figure in different colors.
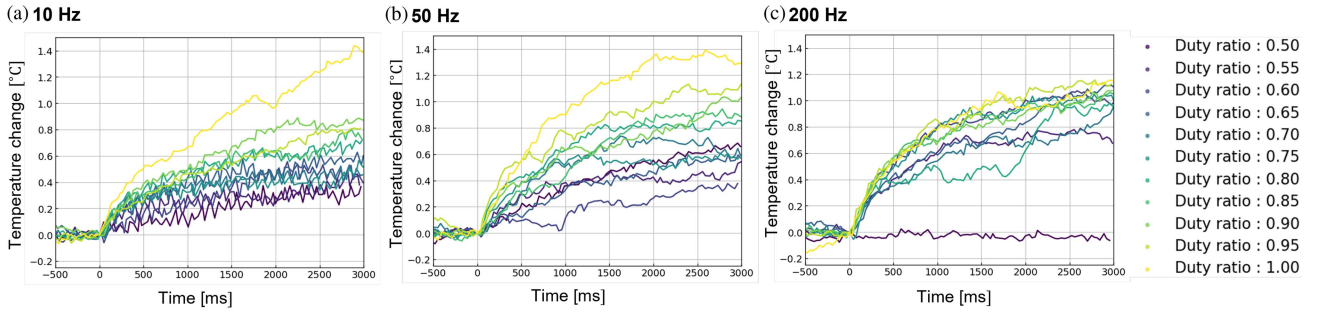

Fig. 12. Temperature change at the focal point in square wave amplitude modulation. Ultrasound was irradiated at $t = 0$ s. Modulation frequencies are (a) 10 Hz, (b) 50 Hz, and (c) 200 Hz. The temperature change at each duty ratio is plotted simultaneously.

waveform. When modulating the static focus with RMS of 5.5 kPa, a significant temperature increase occurs when the duty ratio is 0.55 or higher. Thus, when the measurement and vibrotactile presentation are performed simultaneously, rectangular modulation, instead of sinusoidal modulation, enables focal-point measurement with thermal imaging, even at low sound pressure.

The RMS values at each sound pressure were compared. For static pressure, measurement was possible at 4.0 kPa in 9 out of 10 participants. In the case of the sine wave, measurement was not possible even at a maximum output of 3.1 kPa. The square wave could not be measured at 3.9 kPa but could be measured at 4.1 kPa. These results indicate that a stable measurement is possible as long as the RMS value is 4.1 kPa or higher. The sensitivity of the thermography camera is considered to be a factor that influences these numerical results, but since body temperature fluctuations are larger than the sensitivity of the camera, the results are considered to be almost unchanged.

We believe that the use of static pressure is sufficient for the prior correction of the focus position. In contrast, focus measurement with amplitude modulation is effective when the focus position needs to be corrected while a vibrotactile sensation is being presented or when the focus position is shifted owing to modulation. Square-wave modulation is better used in situations where a shorter measurement time is required, such as in the real-time calibration of the focus position based on the measurement results.

VIII. EXPERIMENT 6: MEASUREMENT OF FOCUS MOVEMENT

Moving foci have been used in aerial tactile presentations to enhance perceptual intensity [15], [16], [17] and to convey directions and symbols [30], [31], [32], [33]. In this section, we evaluate the performance of moving foci in measuring the focal positions and their trajectories.

A. Procedure

The experiment was conducted on palms stimulated by a moving focus in previous studies [13], [15], [16], [17], [31]. Temperature changes were measured by thermal imaging when a moving focal point with a circular orbit of 8 mm radius was presented, and 11 different moving velocities (1, 3, 5, 10, 50, 100, 500, 1000, 2000, 10000, and 20000 mm/s) were used. The RMS sound pressure at the focal point measured using a microphone was 5.5 kPa. During the experiment, the room temperature and humidity were 26.5°C and 59.1%, respectively.

B. Results and Discussion

The thermal images of the focal point at each speed in half and complete orbit are shown in Fig. 13. The largest temperature change in the thermal image is marked with a square. Fig. 13 shows that a temperature change at the focal point can be observed up to 100 mm/s. However, as the velocity increases, the temperature change decreases. At speeds greater than
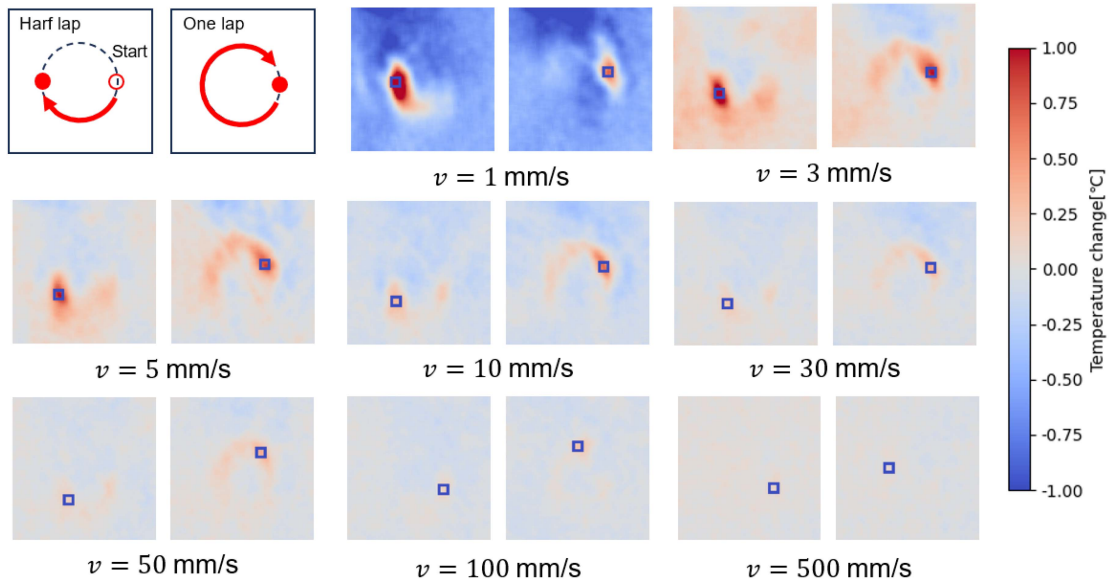
Fig. 13. Distribution of temperature change at half and full cycle as a function of focus velocity, showing that the focal point can be tracked with almost no delay up to $v = 30$ m/s. The square in the figure represents the largest point and was added to convey intuitively the shift between the temperature peak and the sound pressure peak. The square in the figure represents the point where the temperature change is the largest.
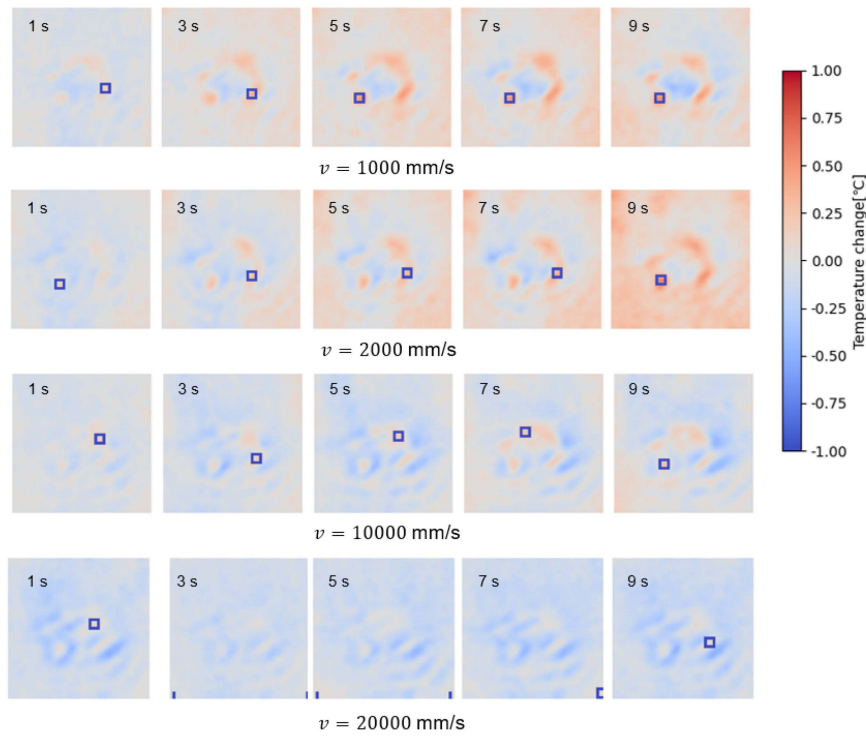
Fig. 14. Distribution of temperature change over time at different moving speeds. It can be seen that the orbit becomes obscured as the speed increases.

500 mm/s, no temperature increase was observed. Applying this measurement to a moving focus at 90 mm/s, as used in a dynamic pointer [31], allows correction of the trajectory. However, based on our results, measuring a focus with a velocity of 100 mm/s would require a sound pressure of approximately 5.5 kPa, thus,

a lower velocity would be required for measurement at a lower sound pressure.

As shown in Fig. 13, measuring the focal point of a free trajectory above 500 mm/s is difficult. However, it is possible to measure the trajectory in a closed-loop situation. Fig. 14

shows the thermal images after 1, 3, 5, 7, and 9 s at speeds above 1000 m/s. An increase in temperature was observed at 10000 mm/s, but the orbit collapsed. and at 20000 mm/s, a temperature increase was observed, but a circular orbit could not be observed. Because the velocity with the highest perceived intensity is between 2000 and 20000 mm/s [15], [16], [17], 2000 mm/s is considered a good velocity for tactile presentation while measuring the orbit.

One possible cause for the orbit not being visualized as the velocity increases is the reduction in sound pressure owing to phase switching [34]. The RMS values of the sound pressure at a certain point on the orbit at each velocity were measured with a microphone. The RMS values decreased by 94% and 87% at $v=10000$ and 20000 mm/s, respectively, compared to 1000 mm/s. It is possible that this was the reason for failure to visualize the sound pressure.

IX. CONCLUSION

In this study, we evaluated the performance of focal position measurements on a finger using thermal imaging. The measurement performance of the ultrasound focus generated by the ultrasound-phased array was experimentally verified. By comparing the microphone sound pressure and the temperature distribution on the silicone surface, we confirmed that the temperature change peak and the sound pressure peak matched within 1.5 mm on the flat and sloping surfaces. Furthermore, even on the curved surface, it was confirmed that they matched within 0.25 mm in the direction along the surface, but deviated by 2.3 mm in the direction perpendicular to the surface.

We also confirmed that the ultrasound focus can be measured with a precision of less than 1 mm on a human finger, with a measurement time of 0.2 s. We found that the unmodulated focus could be measured within 1.6 s at 4.0 kPa for 9 out of 10 participants. When measuring the amplitude-modulated focus, modulating the waveform into a rectangular waveform instead of a sinusoidal waveform was found to be effective. The moving focal point can be measured at velocities of 100 mm/s or less, and the trajectory can be visualized at velocities up to 2000 mm/s.

Repeated measurement and correction of the focal point by thermal image measurement enables the optimization of the sound field in the workspace. The correction of ultrasound focuses on the millimeter scale, which is difficult to achieve with conventional measurement methods, will considerably improve the airborne haptics experience for basic research and practical applications. In the future, a real-time haptic feedback control that tracks a user's finger using the measured focus position is expected to be realized.

ACKNOWLEDGMENT

REFERENCES

[1] I. Rakkolainen, E. Freeman, A. Sand, R. Raisamo, and S. Brewster, "A survey of mid-air ultrasound haptics and its applications," *IEEE Trans Haptics.*, vol. 14, no. 1, pp. 2–19, Jan.–Mar. 2021.

[2] O. Georgiou, W. Frier, E. Freeman, C. Pacchierotti, and T. Hoshi, *Ultrasound Mid-Air Haptics for Touchless Interfaces*. Cham, Switzerland: Springer, 2022.

[3] T. Hoshi, M. Takahashi, T. Iwamoto, and H. Shinoda, "Noncontact tactile display based on radiation pressure of airborne ultrasound," *IEEE Trans Haptics.*, vol. 3, no. 3, pp. 155–165, Jul.–Sep. 2010.

[4] T. Carter, S. A. Seah, B. Long, B. Drinkwater, and S. Subramanian, "UltraHaptics: Multi-point mid-air haptic feedback for touch surfaces," in *Proc. 26th Annu. ACM Symp. User Interface Softw. Technol.*, 2013, pp. 505–514.

[5] T. Howard, G. Gicquel, C. Pacchierotti, and M. Marchal, "Can we effectively combine tangibles and ultrasound mid-air haptics? A study of acoustically transparent tangible surfaces," *IEEE Trans. Haptics*, vol. 16, no. 4, pp. 477–483, Oct.–Dec. 2023.

[6] L. Mulot et al., "DOLPHIN: A framework for the design and perceptual evaluation of ultrasound mid-air haptic stimuli," in *Proc. ACM Symp. Appl. Perception*, 2021, pp. 1–10.

[7] T. Howard, G. Gallagher, A. Lécuyer, C. Pacchierotti, and M. Marchal, "Investigating the recognition of local shapes using mid-air ultrasound haptics," in *Proc. IEEE World Haptics Conf.*, 2019, pp. 503–508.

[8] A. Matsubayashi, Y. Makino, and H. Shinoda, "Direct finger manipulation of 3D object image with ultrasound haptic feedback," in *Proc. CHI Conf. Hum. Factors Comput. Syst.*, 2019, pp. 1–11.

[9] V. Shen, C. Shultz, and C. Harrison, "Mouth haptics in VR using a headset ultrasound phased array," in *Proc. CHI Conf. Hum. Factors Comput. Syst.*, 2022, pp. 1–14.

[10] A. Jingu, T. Kamigaki, M. Fujiwara, Y. Makino, and H. Shinoda, "Lip-Notif: Use of lips as a non-contact tactile notification interface based on ultrasonic tactile presentation," in *Proc. 34th Annu. ACM Symp. Interface Softw. Technol.*, 2021, pp. 13–23.

[11] Y. Monnai, K. Hasegawa, M. Fujiwara, K. Yoshino, S. Inoue, and H. Shinoda, "HaptoMime: Mid-air haptic interaction with a floating virtual screen," in *Proc. 27th Annu. ACM Symp. Interface Softw. Technol.*, 2014, pp. 663–667.

[12] Y. Makino, Y. Furuyama, S. Inoue, and H. Shinoda, "HaptoClone (haptic-optical clone) for mutual tele-environment by real-time 3D image transfer with midair force feedback," in *Proc. CHI Conf. Hum. Factors Comput. Syst.*, San Jose, CA, USA, 2016, vol. 16, pp. 1980–1990.

[13] S. Suzuki, M. Fujiwara, Y. Makino, and H. Shinoda, "Midair hand guidance by an ultrasound virtual handrail," in *Proc. IEEE World Haptics Conf.*, 2019, pp. 271–276.

[14] D. Pittera, O. Georgiou, A. Abdouni, and W. Frier, "'I can feel it coming in the hairs tonight': Characterising mid-air haptics on the hairy parts of the skin," *IEEE Trans. Haptics*, vol. 15, no. 1, pp. 188–199, Jan.–Mar. 2022.

[15] W. Frier et al., "Using spatiotemporal modulation to draw tactile patterns in mid-air," in *Proc. Int. Conf. Hum. Haptic Sens. Touch Enabled Comput. Appl.*, 2018, pp. 270–281.

[16] R. Takahashi, K. Hasegawa, and H. Shinoda, "Lateral modulation of midair ultrasound focus for intensified vibrotactile stimuli," in *Proc. Int. Conf. Hum. Haptic Sens. Touch Enabled Comput. Appl.*, 2018, pp. 276–288.

[17] R. Takahashi, K. Hasegawa, and H. Shinoda, "Tactile stimulation by repetitive lateral movement of midair ultrasound focus," *IEEE Trans. Haptics*, vol. 13, no. 2, pp. 334–342, Apr.–Jun. 2020.

[18] S. Mizutani, M. Fujiwara, Y. Makino, and H. Shinoda, "Thresholds of haptic and auditory perception in midair facial stimulation," in *Proc. IEEE Int. Symp. Haptic, Audio Vis. Environ. Games*, 2019, pp. 1–6.

[19] A. Jingu, M. Fujiwara, Y. Makino, and H. Shinoda, "Tactile perception characteristics of lips stimulated by airborne ultrasound," in *Proc. IEEE World Haptics Conf.*, 2021, pp. 607–612.

[20] A. Abdouni, R. Clark, and O. Georgiou, "Seeing is believing but feeling is the truth: Visualising mid-air haptics in oil baths and lightboxes," in *Proc. Int. Conf. Multimodal Interaction*, 2019, pp. 504/505.

[21] M. Fujiwara, Y. Someya, Y. Makino, and H. Shinoda, "Reflection pattern sensing for valid airborne ultrasound tactile display," in *Proc. IEEE World Haptics Conf.*, 2021, pp. 121–126.

[22] R. Onishi et al., "Two-dimensional measurement of airborne ultrasound field using thermal images," *Phys. Rev. Appl.*, vol. 18, no. 4, 2022, Art. no. 044047.

[23] S. Iwabuchi, R. Onishi, S. Suzuki, T. Kamigaki, Y. Makino, and H. Shinoda, "Performance evaluation of airborne ultrasound focus measurement using thermal imaging on the surface of a finger," in *Proc. IEEE World Haptics Conf.*, 2023, pp. 210–215.

[24] N. Ludwig, D. Formenti, M. Gargano, and G. Alberti, "Skin temperature evaluation by infrared thermography: Comparison of image analysis methods," *Infrared Phys. Technol.*, vol. 62, pp. 1–6, 2014.

[25] E. Staffa et al., "Infrared thermography as option for evaluating the treatment effect of percutaneous transluminal angioplasty by patients with peripheral arterial disease," *Vascular*, vol. 25, no. 1, pp. 42–49, 2017.

[26] A. Moliné et al., "The mental nose and the pinocchio effect: Thermography, planning, anxiety, and lies," *J. Invest. Psychol. Offender Profiling*, vol. 15, no. 2, pp. 234–248, 2018.

[27] K. Mutlu, J. E. Rabell, P. M. Del Olmo, and S. Haesler, "IR thermography-based monitoring of respiration phase without image segmentation," *J. Neurosci. Methods*, vol. 301, pp. 1–8, 2018.

[28] S. Suzuki, S. Inoue, M. Fujiwara, Y. Makino, and H. Shinoda, "AUTD3: Scalable airborne ultrasound tactile display," *IEEE Trans Haptics*, vol. 14, no. 4, pp. 740–749, Oct.–Dec. 2021.

[29] M. Nakajima, K. Hasegawa, Y. Makino, and H. Shinoda, "Spatiotemporal pinpoint cooling sensation produced by ultrasound-driven mist vaporization on skin," *IEEE Trans. Haptics*, vol. 14, no. 4, pp. 874–884, Oct.–Dec. 2021.

[30] L. Mulot, G. Gicquel, W. Frier, M. Marchal, C. Pacchierotti, and T. Howard, "Curvature discrimination for dynamic ultrasound mid-air haptic stimuli," in *Proc. IEEE World Haptics Conf.*, 2021, p. 1145.

[31] D. Hajas, D. Pittera, A. Nasce, O. Georgiou, and M. Obrist, "Mid-air haptic rendering of 2D geometric shapes with a dynamic tactile pointer," *IEEE Trans. Haptics*, vol. 13, no. 4, pp. 806–817, Oct.–Dec. 2020.

[32] L. Mulot, T. Howard, C. Pacchierotti, and M. Marchal, "Ultrasound mid-air haptics for hand guidance in virtual reality," *IEEE Trans. Haptics*, vol. 16, no. 4, pp. 497–503, Oct.–Dec. 2023.

[33] A. Yoshimoto, K. Hasegawa, Y. Makino, and H. Shinoda, "Midair haptic pursuit," *IEEE Trans. Haptics*, vol. 12, no. 4, pp. 652–657, Oct.–Dec. 2019.

[34] S. Suzuki, M. Fujiwara, Y. Makino, and H. Shinoda, "Reducing amplitude fluctuation by gradual phase shift in midair ultrasound haptics," *IEEE Trans. Haptics*, vol. 13, no. 1, pp. 87–93, Jan.–Mar. 2020.

Ryoya Onishi received the M.S. degree from the Department of Complexity Science and Engineering, The University of Tokyo, Chiba, Japan, in 2022, where he has been working toward the Ph.D. degree with the Graduate School of Frontier Sciences, since 2017. His research interests include haptics, ultrasound midair haptics, and human-computer interaction.

Sota Iwabuchi received the B.S. degree from the Department of Applied Physics, Waseda University, Shinjuku, Japan, in 2022. Since 2022, he has been working toward the M.S. degree with the Graduate School of Frontier Sciences, The University of Tokyo, Chiba, Japan. His research interests include haptics, ultrasound midair haptics, and human-computer interaction.

Shun Suzuki received the B.S. degree in physics from Waseda University, Shinjuku, Japan, in 2017, and the M.S. and Ph.D. degrees in complexity science and engineering from The University of Tokyo, Chiba, Japan, in 2019 and 2022, respectively. He is currently a Project Assistant Professor with The University of Tokyo. His research focuses on mid-air haptics.

Takaaki Kamigaki received the B.S. degree and M.S. degrees in engineering from Kumamoto University, Kumamoto, Japan, in 2014 and 2016, respectively, and the Ph.D. degree from The University of Tokyo, Chiba, Japan, in 2019. He is currently a Project Assistant Professor with The University of Tokyo. His research focuses on mid-air haptics.

Yasutoshi Makino received the Ph.D. degree in information science and technology from the University of Tokyo, Tokyo, Japan, in 2007. From 2007 to 2013, he was a Researcher for two years with the University of Tokyo, and an Assistant Professor with Keio University, Minato, Japan. In 2013, he was with the University of Tokyo as a Lecturer, where he has been an Associate Professor, since 2017. He is currently an Associate Professor with the Department of Complexity Science and Engineering, University of Tokyo. His research focuses on haptic interactive systems.

Hiroyuki Shinoda (Member, IEEE) He received the Ph.D. degree in engineering from The University of Tokyo, Chiba, Japan. From 1995 to 1999, he was an Associate Professor with the Tokyo University of Agriculture and Technology, Fuchu, Japan, a Visiting Scholar with UC Berkeley, Berkeley, CA, USA, in 1999, and an Associate Professor with The University of Tokyo, from 2000 to 2012. He is currently a Professor with the Graduate School of Frontier Sciences, The University of Tokyo. His research interests include information physics, haptics, mid-air haptics, two-dimensional communication, and their application systems. He is a member of *SICE, IEEJ, RSJ, JSME, VRSJ*, and *ACM*.